Hindawi
International Journal of Antennas and Propagation
Volume 2023, Article ID 9754710, 1 page
https://doi.org/10.1155/2023/9754710

Retraction

Retracted: A DSP-Controlled Permanent Magnet Synchronous Motor Control System for Hybrid Vehicles

International Journal of Antennas and Propagation

Received 19 December 2023; Accepted 19 December 2023; Published 20 December 2023

This article has been retracted by Hindawi following an investigation undertaken by the publisher [1]. This investigation has uncovered evidence of one or more of the following indicators of systematic manipulation of the publication process:

(1) Discrepancies in scope

(2) Discrepancies in the description of the research reported

(3) Discrepancies between the availability of data and the research described

(4) Inappropriate citations

(5) Incoherent, meaningless and/or irrelevant content included in the article

(6) Manipulated or compromised peer review

The presence of these indicators undermines our confidence in the integrity of the article's content and we cannot, therefore, vouch for its reliability. Please note that this notice is intended solely to alert readers that the content of this article is unreliable. We have not investigated whether authors were aware of or involved in the systematic manipulation of the publication process.

Wiley and Hindawi regrets that the usual quality checks did not identify these issues before publication and have since put additional measures in place to safeguard research integrity.

We wish to credit our own Research Integrity and Research Publishing teams and anonymous and named external researchers and research integrity experts for contributing to this investigation.

The corresponding author, as the representative of all authors, has been given the opportunity to register their agreement or disagreement to this retraction. We have kept a record of any response received.

References

[1] Q. Fu, "A DSP-Controlled Permanent Magnet Synchronous Motor Control System for Hybrid Vehicles," *International Journal of Antennas and Propagation*, vol. 2022, Article ID 1996502, 9 pages, 2022.

Hindawi
International Journal of Antennas and Propagation
Volume 2022, Article ID 1996502, 9 pages
https://doi.org/10.1155/2022/1996502

Research Article

A DSP-Controlled Permanent Magnet Synchronous Motor Control System for Hybrid Vehicles

Qiang Fu [1,2]

[1]*Shenyang Aerospace University, Shenyang, Liaoning 110136, China*
[2]*Liaoning General Aviation Research Institute, Shenyang, Liaoning 110136, China*

Correspondence should be addressed to Qiang Fu; fuqiang@sau.edu.cn

Received 17 May 2022; Revised 27 May 2022; Accepted 17 June 2022; Published 4 July 2022

Academic Editor: Tao Cui

Compared with other motors, the permanent magnet synchronous motor (PMSM) is small and occupies less space. At the same time, its weight is relatively light, so it is more in line with the development trend of hybrid electric vehicle (EV) drive motor lightweight miniaturization and has been widely used. This article studies a DSP-controlled PMSM control system for hybrid vehicles. Firstly, the motor drive control system is mainly controlled by DSP2812 chip. Then, a maximum torque current ratio control method was proposed to optimize the energy efficiency of hybrid vehicles based on PMSM. The longitudinal dynamic model of the moving hybrid vehicle was obtained by force analysis. Combined with the basic equation of PMSM and the transmission system of the hybrid vehicle, the mathematical model of PMSM-EV was established. The experimental results show that the maximum torque current ratio control method applied to hybrid vehicles can effectively reduce the loss, improve the efficiency and dynamic performance, and solve the endurance problem of hybrid vehicles to a certain extent. This advantage is significant in the dynamic acceleration and deceleration of hybrid vehicles.

1. Introduction

As the most classical control technologies of PMSM, FOC and DTC are widely used at present [1]. However, FOC is too dependent on motor parameters and the steady-state torque pulsation of DTC is too large, which cannot meet the high precision control requirements of PMSM [2]. The dynamic performance of SMC is good, but the chattering problem cannot be solved effectively, resulting in mechanical loss of PMSM [3]. The future of predictive control and intelligent control is very promising. The advantages of PMSM are far from replacing other motors in the current competitive market environment [4].

For PMSM, its flux material is a permanent magnet. The magnetic flux direction represents axis d, and the axis perpendicular to the magnetic flux direction is axis q [5]. When the q-axis current can meet the requirements of the left-hand rule, the current belongs to the q-axis current [6]. Compared with the induction motor and the q-axis current, to ensure sufficient flux, there should also be a current in the d-axis direction, which belongs to the d-axis current. Therefore, the permanent magnet motor only needs less current to achieve the torque required for operation, effectively reducing operation loss [7]. More attention is paid to the motor drive system with higher operation efficiency in the research and development of electric vehicles. Based on the actual structure, the permanent magnet motor shows two characteristics. First, rotor permanent magnets can select built-in modes. Second, it can carry out multi-pole design [8]. The motor control system will inevitably develop toward smaller volume and lighter weight, and motor drive performance and operation performance will be further improved.

In this paper, a field weakening control strategy for electric vehicles with torque as the control target is proposed [9]. The maximum torque curve and strategy switching torque curve of the motor were obtained by off-line calculation. According to the feedback speed and target torque, the motor's weak magnetic working point is constantly updated to make it move in a certain area [10]. Thus, the

motor's torque response speed and operation efficiency are improved under complex operating conditions. The feasibility and performance advantage of the whole control strategy are verified by Matlab/Simulink simulation [11]. However, the Tmax and TP strategy switching curves used in this strategy are calculated by the actual motor parameters, so the motor parameters are not considered.

The maximum torque per ampere control method for hybrid vehicles was proposed [12]. The given value of motor drive current in this method is a nonlinear function of hybrid vehicle load, and the optimal given value of straight-axis current I_d and cross-axis current I_q can be obtained through the numerical solution. The proposed method is compared with the traditional other control methods under different external resistance and vehicle speed [13]. A maximum torque current ratio control method was proposed to aim at the energy efficiency optimization of hybrid vehicles based on PMSM. The longitudinal dynamic model of the hybrid vehicle was obtained by force analysis [14]. Combined with the basic equation of PMSM under *d-q* axis and the transmission system of the hybrid vehicle, the overall mathematical model of PMSM-EV was established [15]. But in this article, only the copper loss of the motor is optimized, without considering the influence of the motor iron loss, stray loss, reverse loss, transmission loss, and so on [16].

The mathematical model was first established and the maximum torque current ratio control was proposed at a low speed [17]. The current control strategy of full speed domain controlled by a weak magnetic field is adopted at medium and high speed, and the mathematical model of solving each control is analyzed [18]. Then, the mathematical model is discretized and the state space equation is obtained. Based on this, the speed controller of model predictive control and the current controller of beat-free predictive control are designed [19]. Predictive control is used to replace the traditional double-loop PI control. When the speed step is set, the speed response of the motor is fast and there is no overshoot. At the same time, the anti-load disturbance ability and recovery ability are better than the traditional double-ring PI controller. By limiting the torque increment, different acceleration modes can be realized to meet the different requirements of drivers for vehicle power and comfort.

Hybrid vehicles have broad development prospects. For the motor control system of hybrid vehicles, the current research and development are fundamental. In this article, DSP2812 chip is selected to build the PMSM control system. To improve the energy efficiency of PMSM hybrid vehicles, this article adopts the maximum torque current ratio control method for the motor control system. The longitudinal dynamic model of a hybrid vehicle was obtained by force analysis. Combined with the PMSM equation and the transmission system of the hybrid vehicle, the overall mathematical model of PMSM-EV was established. It is found that the new system can improve the accuracy of the control system when it is affected by parameter changes or external disturbances. At the same time, the ripple of flux and torque can be reduced and the accuracy of direct torque control can be enhanced. Comparing the improved system with the traditional motor control system, the feasibility and effectiveness of the control algorithm designed in this article are verified.

This article consists of four main parts: the first part is the introduction, the second part is the methodology, the third part is the result analysis and discussion, and the fourth part is the conclusion.

2. Methodology

2.1. System Hardware Circuit Design. The motor drive control system mainly uses DSP2812 chip to control each device. The driving part of power is driven by an IPM inverter so that the motor can work normally. Figure 1 shows the overall architecture of the motor control system.

The hardware architecture of the system is mainly divided into two parts. One part is the control hardware circuit and the other part is the power drive hardware circuit. In addition, the auxiliary circuit includes a power supply circuit and a signal detection circuit. Considering that the control circuit is susceptible to interference from the high voltage side of the power drive circuit during operation, the system architecture adds an optocoupler isolation circuit at the junction of the two parts of the circuit. The system controls the running state of the motor according to the command of signal acquisition. processor is added to the system, and TMS320F2812 is selected as the core control chip. For the application of the inverter, the internal power switch is the main control device. By adjusting the current amplitude and frequency, the current flow in the circuit is converted to a three-phase AC power supply, to drive the motor to work normally.

2.1.1. Main Power Circuit Design. This system uses MOSFET power tube IRF2807, which can get a faster switching speed, especially suitable for driving a small power motor. There is a reverse quick recovery diode integrated between the drain and source poles inside the motor, which can directly protect the MOS tube without an external connection. The bypass resistor R is used to measure the current on the DC bus of the motor. The current signal I is measured by the voltage drop of resistance R. The current signal can provide a feedback current signal for the current loop. At the same time, the current signal can be real-time monitoring current to prevent motor overcurrent failure. The overcurrent signal is input into the front driver chip and DSP processor of the power bridge, and the gate driver signal of the power field effect tube is blocked in time during overcurrent.

To improve the safety performance of system operation, this design scheme adds an inverter circuit to the system hardware architecture, PS21865 as the controller, design inverter circuit.

Because the PWM waveform generated by DSP has a high frequency (33 kHz), the switching time of the driving circuit will be longer with the general low-speed optocoupler, and the low-speed performance of the motor will be seriously affected at low speed and small load. Therefore, high-speed optocoupler 6N137 is selected in this article. The

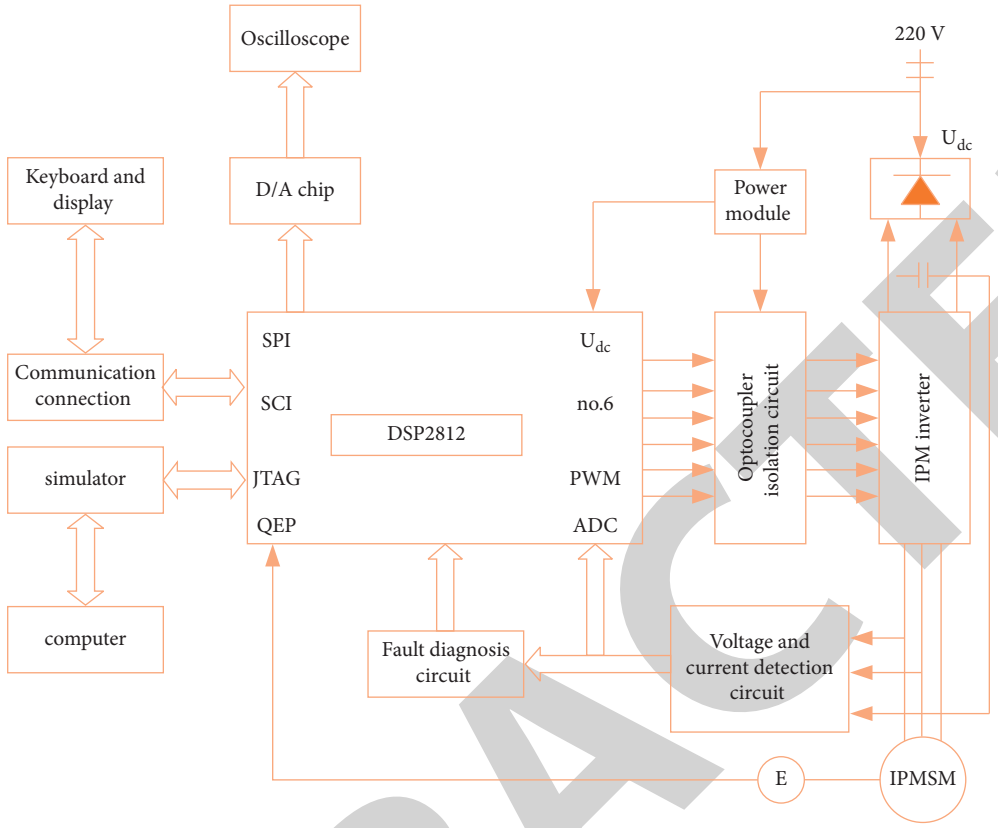

Figure 1: Overall architecture of motor control system.

maximum switching speed of the optocoupler is 10 MHz, which effectively improves the rapidity of the inverter.

2.1.2. Signal Detection Circuit Design. The three-phase stator voltage of the system, namely the U, W, and V phases, needs to be calculated according to the detection of DC bus voltage and the observation of the current inverter switch operation state. Considering that the voltage in the circuit is dc voltage, the system adopts the method of resistance voltage division to collect voltage information. The circuit sets the value of divider resistance in the limited range of DC bus voltage. The former is the power resistor and the latter is the patch resistor. To improve the impedance performance and isolation function of the circuit, a voltage follower is added after the voltage divider circuit, which works together with the analog photoelectric coupler to adjust the isolation signal in the circuit. The output signal of the circuit is an analog signal, after A/D conversion processing, the digital signal is generated, and TMS320F2812 calculates the signal data.

TMS320F2812 chip contains 12-bit unipolar A/D conversion module. The minimum conversion time is 60 ns, which can realize the three-phase voltage sampling of the motor without phase compensation. But because it is unipolar, we should add a lifting circuit when sampling AC, so that the voltage range of the AC signal is between 0 and 3 V. This system uses three A/D conversion inputs, two current detections, and one analog signal input sampling. Because of the balance between the three phases of the system, so as long as the detection of two currents, we can get the three-phase current. In the system, the hall current sensor is used to detect the motor stator current, and the input-output ratio is 200:1. The hall current sensor outputs weak current signals, which are converted into voltage signals, and then filtered and added. To prevent the voltage from being too high or too low, a limiting circuit composed of diodes is designed.

The current detection circuit is the biggest advantage of high precision measurement, good linearity, and can do no contact detection.

The protection circuit includes the overcurrent, overvoltage, and undervoltage of the main circuit as well as the fault signals such as overload and short circuit. To ensure the safe and reliable work of the power conversion circuit and motor drive circuit in the system, TMS320F2812 provides a PDPPINT input signal, which can be used to realize various protection functions of the control system conveniently.

Although IPM has a fully functional protection circuit, it still requires that the drive signal be removed in the event of power device failure. After IPM outputs four fault signals "or" to each other, they pass through the low-pass filter and serve as the protection signal of the DSP power device. At the same time, the guard signal controls the bus driver and immediately shuts down the drive signal sent to the rear stage when the fault signal is effective. With this dual protection design, the reliability of the system is further improved. The fault detection circuit is three fault output signals of the upper bridge arm of IPM, and the driving

power supply is isolated from each other. The three fault signals of the lower bridge arm are combined into one. Since there is no fault memory unit in IPM, the external control system needs to process its fault signal and take corresponding measures to completely block the IPM drive signal to ensure the safety of IPM. The fault detection module can complete the main circuit fault signal acquisition, and feedback to the control system, the control system according to the fault state to make a judgment and give the corresponding treatment scheme. The fault detection module collects the fault signal of the main loop and feeds back to the control system. Its function is to feedback fault signal in time, optimize the model, protect the circuit, and reduce the loss.

2.1.3. System Power Supply Circuit Design. First, the DC power supply is selected for the operation of each module in the system. To avoid mutual interference of power supply, the power supply of the system is isolated from each other. According to the rated voltage of the equipment, the power supply circuit is equipped, respectively. In this design, LM2576 is selected as the core chip of the circuit power supply, which supports 24 to 5 V power supply. Under the joint action of F2415S-2W equipment, the conversion between 24 V DC and 15 V DC is realized. Considering the power supply-demand of other equipment in the hardware circuit of the system, the WRA2412YMD-6W module is also added to the circuit, which provides ±12V power supply to each equipment with this model. Considering that some lines need partial voltage, this design scheme selects TMS320 F2812 as the control device, and the line supply voltage range is 1.9 and 3.3 V. The core chip of the control device is TPS767D301. Under the action of this chip, the power supply voltage is split into two channels, which are adjustable voltage (range 1.5~5.5 V) and fixed voltage 3.3 V, respectively. The line voltage is controlled by switching pin high/low level by adjusting the supply sequence.

2.2. Improved DTC Control Scheme

2.2.1. Establishment of Mathematical Model of PMSM. Since PMSM is not a linear system, the mathematical model of PMSM should be established if the control algorithm is used to achieve accurate control of PMSM. For PMSM, its flux material is a permanent magnet. The magnetic flux direction represents axis d, and the axis perpendicular to the magnetic flux direction is axis q. The relationship between coordinate systems of the mathematical model of PMSM is shown in Figure 2.

Formula (1) is the stator voltage equation of PMSM in a synchronous rotation coordinate system.

$$\begin{cases} u_d = Ri_d + \dfrac{\mathrm{d}}{\mathrm{d}t}\psi_d - \omega_e\psi_q, \\ u_q = Ri_q + \dfrac{\mathrm{d}}{\mathrm{d}t}\psi_q + \omega_e\psi_d. \end{cases} \tag{1}$$

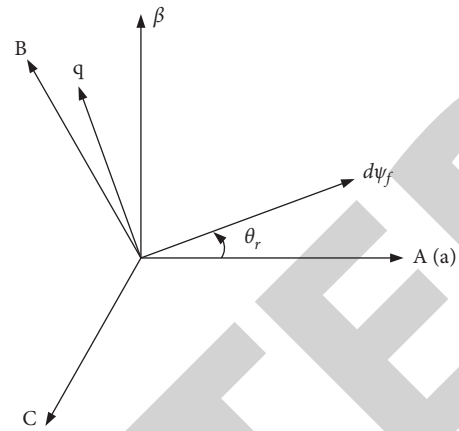

Figure 2: Relationship among coordinate systems.

Formula (2) is the stator flux equation.

$$\begin{cases} \psi_d = L_d i_d + \psi_f, \\ \psi_q = L_q i_q. \end{cases} \tag{2}$$

Formula (3) can be obtained by substituting the stator flux equation with the stator voltage equation.

$$\begin{cases} u_d = Ri_d + L_d\dfrac{\mathrm{d}}{\mathrm{d}t}i_d - \omega_e L_q i_q, \\ u_y = Ri_q + L_q\dfrac{\mathrm{d}}{\mathrm{d}t}i_q + \omega_e\left(L_d i_d + \psi_r\right). \end{cases} \tag{3}$$

When the mathematical model of PMSM is completely decoupled, the electromagnetic torque equation can be obtained.

$$T_e = \frac{3}{2}U_t i_q\left[i_d\left(L_d - L_q\right) + \psi_f\right], \tag{4}$$

where u_d and u_q are the stator voltages on axis d and q. Rs is the stator resistance. ω_e is electric angular velocity. i_d and i_q are the stator currents on axis d and q. ψ_d and ψ_q are the stator flux on axis d and q. ψ_f and U_t are permanent magnet flux and motor pole pairs. L_d and L_q are the inductance coefficients on axis d and q.

2.2.2. The Traditional DTC Control Scheme of PMSM. According to formula (4), DTC control further processes the electromagnetic torque formula to obtain the following formula:

$$T_e = \frac{3pn}{4L_d L_q}\left|\Psi_s\right|\left(2\psi_f L_q \sin\delta + \left|\psi_s\right|\left(L_d - L_q\right)\sin 2\delta\right), \tag{5}$$

where $|\Psi_s|$ is the amplitude of the stator flux. δ is the included angle between flux chains of the fixed rotor, also known as torque angle.

For the selected PMSM, the polar logarithm of the motor, the inductance coefficient of the d q axis, and the permanent magnet flux are constant values. According to formula (5), the only variables in the formula are torque angle and stator flux. When the control stator flux is

constant, that is, the circular magnetic field distribution, then the torque angle is the only variable, and the size of the electromagnetic torque depends on the change of the torque angle, which is the basic principle of the traditional DTC control of PMSM.

2.2.3. DTC Control Principle. The advantage of space pulse-width modulation is that it can synthesize the desired voltage vector at any position and improve the vibration caused by the finite voltage vector transformation in the table lookup method. Combining the advantages of space pulse width modulation with the simple control structure of DTC control technology to improve the flux and torque pulsation and slow response in traditional DTC control, this is the direct torque control principle of space voltage vector. The control system block diagram is shown in Figure 3.

The vector of voltage vector $\mathbf{U}_s$ in T_s is composed of the vector of non-zero voltage vector $\mathbf{U}_4$ in T_4 time and the vector of non-zero voltage vector $\mathbf{U}_6$ in T_6 time. The equivalence principle is shown in formula (6).

$$\begin{cases} T_s\mathbf{U}_s = T_4\mathbf{U}_4 + T_6\mathbf{U}_6, \\ T_s = T_4 + T_6 + T_0, \end{cases} \tag{6}$$

where T_0 represents the effective time of the zero voltage vector. T_s represents a control cycle.

The equivalence principle should be combined with the voltage vector synthesis method. The vector diagram of the voltage vector synthesis method is shown in Figure 4.

In space vector pulse width modulation direct torque control system, flux estimation module and torque estimation module remain unchanged. The expressions of reference voltage vectors U_α^* and U_β^* are shown in the following formula (7)

$$\begin{cases} U_\alpha^* = \dfrac{|\psi_s^*|\cos(\theta + \Delta\theta) - |\psi_s|\cos\theta}{T_s} + R_s i_\alpha, \\ U_\beta^* = \dfrac{|\psi_s^*|\sin(\theta + \Delta\theta) - |\psi_s|\sin\theta}{T_s} + R_s i_\beta. \end{cases} \tag{7}$$

2.2.4. The Influence of Stator Resistance Change on the Control System. In the PMSM control system, the calculation and measurement of stator flux value are troublesome and has low accuracy. One is the direct measurement method, which directly measures the stator flux value through the induction coil arranged inside the motor, but this measurement method is difficult to install, has low measurement accuracy, and has a high cost, so it is seldom used in engineering. The other is the observation model method, which uses a flux observer to obtain the stator flux value indirectly. Although this measurement method is simple and feasible, it needs to detect the change of motor parameter value in real-time. When the motor is at high speed, the flux can be estimated by the voltage model method. At this time, because the stator resistance partial pressure is much smaller than the stator voltage in the order of magnitude, it can be excluded. On the contrary, when the motor is in a low-speed state, the stator voltage change caused by the change of stator resistance value needs to be measured, otherwise, the stator flux measurement will have a large deviation. The flux equation of PMSM is shown in formula (8)

$$\psi_s^* = \int (u_s - R_S i_s)\mathrm{d}t. \tag{8}$$

According to formula (8), when the motor is at low speed, the value of stator resistance R_S affected by temperature changes, resulting in inaccurate flux measurement, thus affecting the normal operation of the motor and the overall control effect.

Theoretically, the stator resistance of the motor will not change, but in practice, when the motor runs at low speed, the increase of motor temperature will lead to the change of stator resistance and current. Assuming that their variations are, respectively, ΔR_S and $\Delta R i_S$, the actual stator flux and electromagnetic torque formula is shown in formula (9)

$$\begin{aligned} \Psi_s &= \int (u_s - (R_s + \Delta R_s)(i_s + \Delta i_s))dt, \\ T_e &= \frac{3}{2}U_t\left[\Psi_\alpha\left(i_\beta + \Delta i_\beta\right) - \Psi_\beta(i_\alpha + \Delta i_\alpha)\right]. \end{aligned} \tag{9}$$

Before the stator resistance changes, the formula of stator flux and electromagnetic torque is shown in formula (10)

$$\begin{aligned} \widehat{\Psi}_s &= \int [u_s - R_s(i_s + \Delta i_s)]dt, \\ \widehat{T}_e &= \frac{3}{2}U_t\left[\widehat{\Psi}_\alpha\left(i_\beta + \Delta i_\beta\right)(i_\alpha + \Delta i_\alpha)\right]. \end{aligned} \tag{10}$$

Thus, the error between stator flux and electromagnetic torque is shown in formula (11)

$$\begin{aligned} \Delta\Psi_s &= \Psi_s - \widehat{\Psi}_s = -\int \Delta R_s(i_s + \Delta i_s)dt, \\ \Delta T_e &= T_e - \widehat{T}_e = \frac{3}{2}U_t\left[\Delta\Psi_\alpha\left(i_\beta + \Delta i_\beta\right) - \Delta\Psi_\beta(i_\alpha + \Delta i_\alpha)\right]. \end{aligned} \tag{11}$$

The measurement error of stator resistance will bring a large deviation to the calculation of stator flux and electromagnetic torque measurement, which leads to large flux and torque pulse width of the whole control system, and seriously affects the accuracy and control performance of the whole control system.

2.3. Stator Resistance Tracker Design. The relationship between stator flux vector, stator current vector, and rotor flux vector in a synchronous rotation coordinate system is shown in Figure 5.

Suppose that ψ_1 and ψ_2 are the actual value and the observed value of stator flux, respectively. Is_1 and Is_2 are the expected current value and their actual value, respectively.

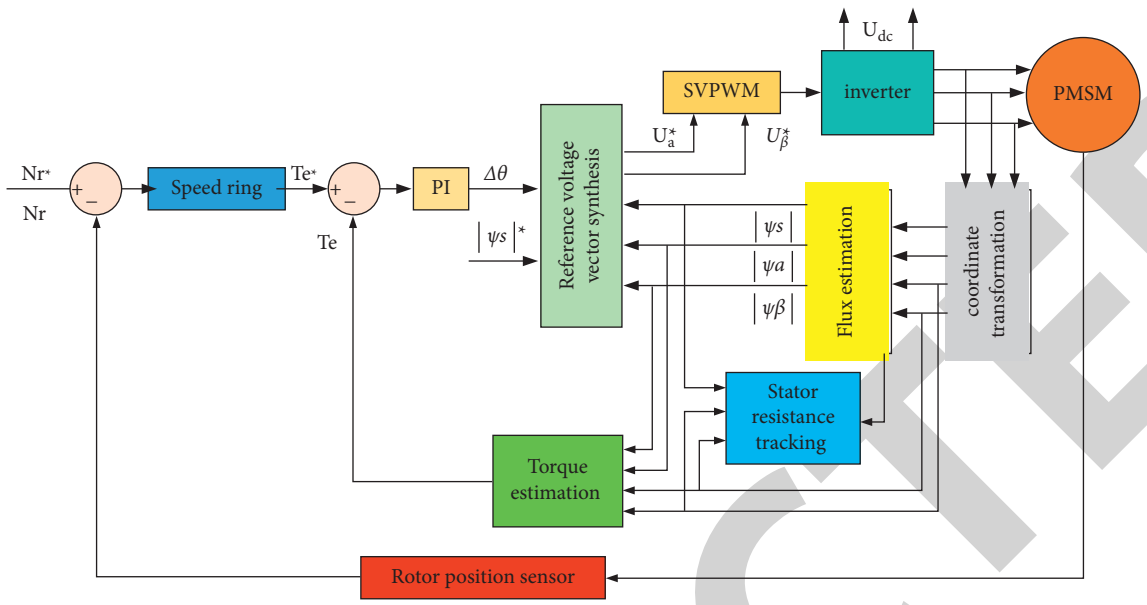

Figure 3: Block diagram of permanent magnet synchronous motor DTC control system with stator resistance tracking.

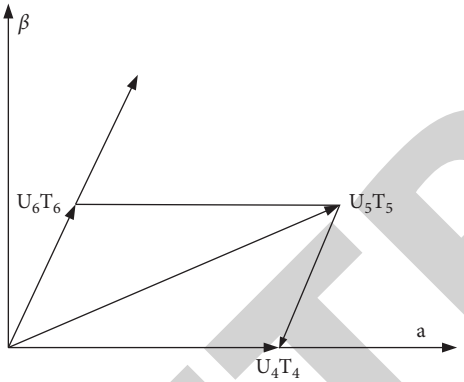

Figure 4: Voltage vector synthesis method.

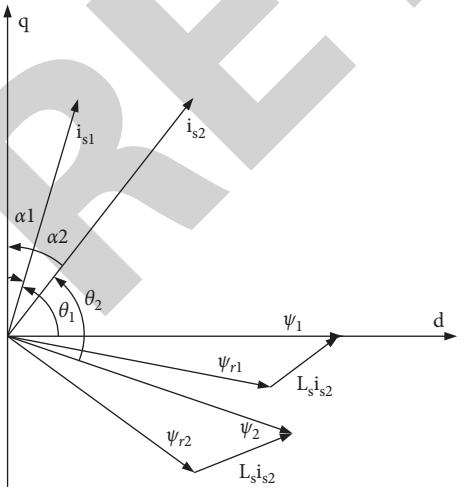

Figure 5: Schematic diagram of flux vector relations.

ψr_1 and ψr_2 are the actual value and the observed value of rotor flux, respectively. According to Figure 5, when the stator resistance value increases, the actual stator flux value should be ahead of the observed value, and the expected current value should be ahead of the actual value.

When the motor is running a steady-state, the flux is distributed according to the circular magnetic field, so the size of the flux is constant. Similarly, when the motor load does not change, the torque generated in the control system remains constant.

$$\begin{cases} |\psi_1| = |\psi_2|, \\ |\psi_1||i_{s1}|\cos\alpha_1 = |\psi_2||i_{s2}|\cos\alpha_2, \\ |\psi_{r1}| = |\psi_{t2}|. \end{cases} \tag{12}$$

Formula (13) can be obtained from trigonometric functions in Figure 5.

$$\begin{aligned} |\psi_{r1}|^2 &= |\psi_1|^2 + |L_s i_1|^2 - 2|\psi_1||L_s i_{,1}|\cos\theta_1, \\ |\psi_n|^2 &= |\psi_2|^2 + |L_s i_2|^2 - 2|\psi_2||L_s i_2|\cos\theta_2. \end{aligned} \tag{13}$$

Formula (14) can be obtained from formula (12) and formula (13).

$$2|\psi_2|\left(\cos\theta_2 - \frac{\cos\alpha 2}{\cos\alpha}\cos\theta_1\right) = |i_{s2}|\left(\frac{\cos\alpha_\alpha 2}{\cos\alpha_1} - 1\right)L_s. \tag{14}$$

Formula (14) is further simplified to formula (15)

$$\frac{|\psi_2|}{|i_{s2}|} = \frac{L_s}{2}\left(\frac{\cos 2_{\alpha 2} - \cos\alpha_{\alpha 1}}{\cos\alpha 1\left(\cos\theta_2\cos\alpha 1 - \cos\alpha_2\cos\theta_1\right)}\right). \tag{15}$$

Let $W = |\psi_2|/|i_{s2}|$, and take the partial derivative of α_2 with respect to W.

$$\frac{\partial W}{\partial \alpha_2} = \frac{L_s\cos\alpha_2}{\cos\alpha_1\cos\theta_1}. \tag{16}$$

According to $\cos\alpha_2 > 0$, W increases with the increase of $\cos\alpha_2 > 0$, resistance changes in the same direction as α_2, and

Table 1: Basic parameters of permanent magnet synchronous motor.

PMSM type	Non-salient pole type	A logarithmic	4
Stator resistance (Ω)	1.2	Dc bus voltage (V)	300
The stator inductance (/mH)	8.6	Rated power (kW)	1.8
Permanent magnet flux (Wb)	0.178	The rated torque (N·m)	6

Table 2: Control system simulation conditions setting.

Parameter	The numerical
Simulation step size and sampling time (t/s)	1e-6
Reference stator flux (Wb)	0.216
The given speed (Nr/(r·min^{-1}))	120
PWM switching frequency (f/Hz)	1000
The simulation time (t/s)	0.2

$\cos\alpha_2 > 0$ decreases with the increase of α_2, so the change direction of W is opposite to resistance. That is, the ratio between the observed value of stator flux and the actual current value is opposite to the direction of resistance change. Therefore, the actual stator resistance value can be measured by using an auxiliary variable flux observation value that changes in the opposite direction of the actual current value and the resistance. Then it passes through the low-pass filter and PI controller successively. Then the stator resistance's compensation amount can be obtained to measure the actual stator resistance value.

3. Result Analysis and Discussion

3.1. Experimental Parameters. In Matlab/Simulink simulation software, the simulation model of the traditional direct torque control system and space vector pulse width modulation DTC system with stator resistance tracking were established according to the above optimization control strategy. The simulation motor in the system adopts the implicit pole permanent magnet synchronous motor, and its basic motor parameters are shown in Table 1.

Simulation conditions are set as shown in Table 2.

3.2. Performance Comparison. The proposed algorithm and the other four control algorithms are compared.

3.2.1. Steady-State Energy Efficiency of Hybrid Vehicles under Different Driving Resistances at a Constant Speed of 28 km/h. Figures 6 and 7 show the simulationresults of the proposed algorithm and other control algorithms [20–23] for hybrid electric vehicles. Figure 6 shows the relationship between the lost power and road driving resistance moment (TR) of hybrid vehicles under the five controllers, and Figure 7 shows the relationship between system efficiency and road driving resistance moment (TR). When the speed is constant, with the increase of external resistance, the power loss of the hybrid vehicle increases gradually, and the system efficiency decreases gradually. When the external resistance is small, the loss of power of the five control methods is close to the system efficiency. With the increase of resistance, the

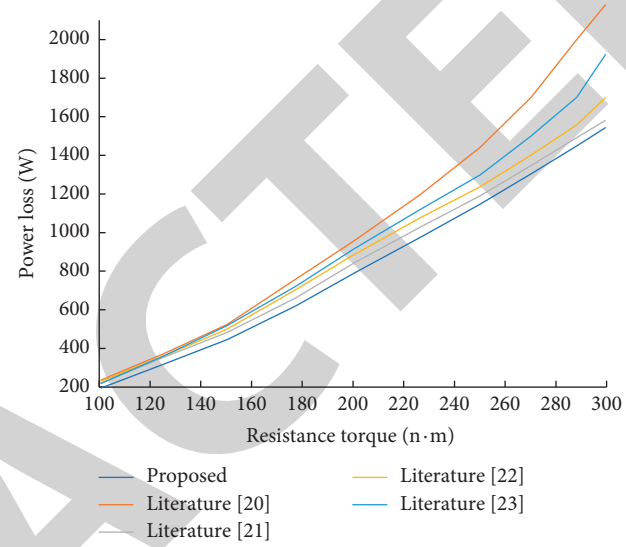

Figure 6: Relationship between lost power and resistance moment.

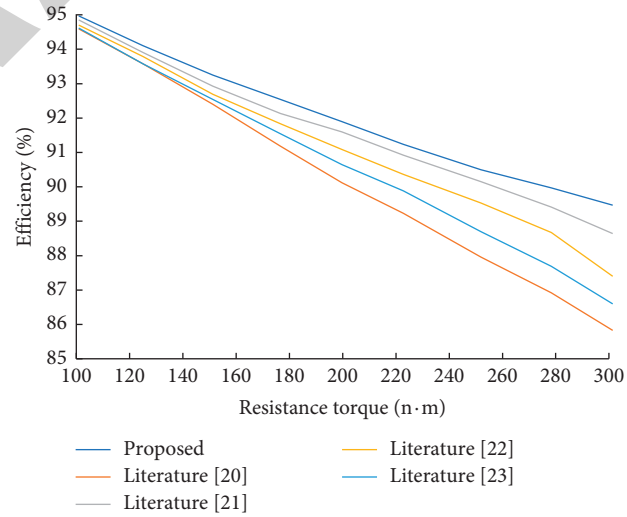

Figure 7: Relationship between system efficiency and resistance moment.

advantages of the proposed control method become more and more apparent. Compared with the other control method, the proposed control method can significantly reduce loss and improve efficiency.

3.2.2. The Steady State Energy Efficiency of Hybrid Vehicles at Different Driving Speeds When the Road Driving Resistance Moment Is Constant at 180 N m. Figures 8 and 9 show the

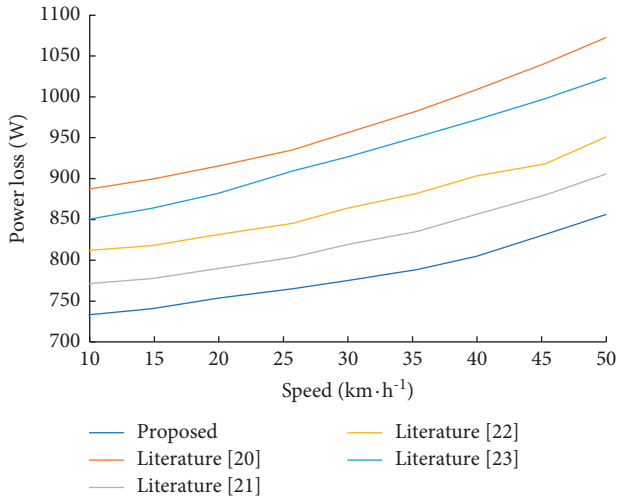

Figure 8: Relationship between lost power and driving speed.

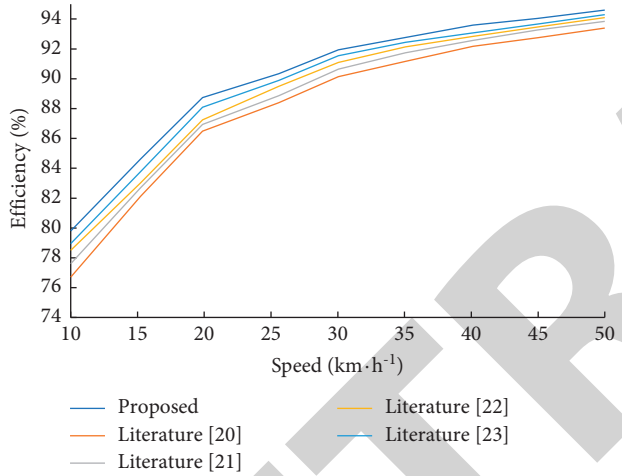

Figure 9: Relationship between system efficiency and driving speed.

simulation results of hybrid vehicles at different speeds. Figure 8 shows the relationship between lost power and driving speed of hybrid vehicles under the five controllers, and Figure 9 shows the relationship between system efficiency and driving speed. It can be seen that the proposed control method has lower loss and higher efficiency than the other control method at different speeds. With the increase in driving speed, the wind resistance gradually increases, and the power loss of the hybrid vehicle under the control of the five methods will rise slightly. However, the loss of power of the proposed method rises more slowly. Since the increase of useful work caused by the increase in speed is much higher than the increase of loss caused by the increase in wind resistance, the efficiency of hybrid vehicles increases gradually with the increase of speed. As the proportion of loss decreases gradually, the efficiency gap between the five methods decreases gradually.

As can be seen from (1) and (2), the performance of the proposed control method is superior to that of the other control method under different speeds and resistance moments. And with the decrease of velocity and the increase of resistance moment, its advantage becomes more and more obvious.

4. Conclusion

The system develops the main power circuit, signal detection circuit, and system power circuit, and reasonably selects the circuit control chip, and builds the hardware circuit for itself. The steady-state error, overshoot, and torque pulsation produced by the system are small. At the same time, the bus voltage output waveform of the system is relatively stable, which meets the requirements of system development. The principle of space voltage vector direct torque control (DTC) combines the advantages of space pulse width modulation (PWM) with the characteristics of the simple control structure of DTC control technology to improve the flux and torque pulsation and slow response speed in traditional DTC control.

This article proposes a maximum torque current ratio control method for energy efficiency optimization of hybrid vehicles based on a permanent magnet synchronous motor (PMSM). The longitudinal dynamic model of a hybrid vehicle was obtained by force analysis. The simulation results show that compared with the traditional zero-axis current control method, this control method can effectively reduce energy consumption and improve the efficiency and performance of the hybrid electric vehicle. This advantage is significant in the dynamic process of acceleration and deceleration of hybrid vehicles. The control strategy studied in this article can solve the endurance problem of hybrid vehicles to a certain extent. The proposed control method has lower loss and higher efficiency than the other control method at different speeds. With the increase of driving speed, wind resistance gradually increases, and the power loss of hybrid vehicles under the control of the two methods rises slightly, but the power loss of the proposed algorithm rises more slowly. The increase in useful work due to the increase in speed is much greater than the increase in loss due to the increase in wind resistance. Therefore, the efficiency of hybrid cars rises gradually with the increase in speed. As the proportion of loss decreases gradually, the efficiency gap between the two methods decreases gradually. The performance of the proposed control method is better than that of the other control method under different speeds and resistance moments, and its advantages become more and more obvious with the decrease in speed and the increase of resistance moments.

However, this article only optimizes the copper loss of the motor without considering the influence of iron loss, stray loss, reverse loss, and transmission loss. It is important research content in the future to integrate various losses on hybrid vehicles and optimize the overall losses.

Data Availability

The labeled data set used to support the findings of this study is available from the corresponding author upon request.

Conflicts of Interest

The author declares that there are no conflicts of interest.

Acknowledgments

This work was supported by the Basic Scientific Research Project of Education Department of Liaoning Province: "Research on Jet Power Brake Dynamics Mechanism and Intelligent Control Strategy of New Energy Flying Vehicle" (No. LJKZ0227).

References

[1] J. Liu, C. Gong, Z. Han, and H. Yu, "IPMSM model predictive control in flux-weakening operation using an improved algorithm," *IEEE Transactions on Industrial Electronics*, vol. 65, no. 12, pp. 9378–9387, 2018.

[2] X. Sun, M. Wu, G. Lei, Y. Guo, and J. Zhu, "An improved model predictive current control for PMSM drives based on current track circle," *IEEE Transactions on Industrial Electronics*, vol. 68, no. 5, pp. 3782–3793, 2020.

[3] Y. Wang, Y. Feng, X. Zhang, and J. Liang, "A new reaching law for antidisturbance sliding-mode control of PMSM speed regulation system," *IEEE Transactions on Power Electronics*, vol. 35, no. 4, pp. 4117–4126, 2019.

[4] D. F. Valencia, R. Tarvirdilu-Asl, C. Garcia, J. Rodriguez, and A. Emadi, "A review of predictive control techniques for switched reluctance machine drives. Part II: torque control, assessment and challenges," *IEEE Transactions on Energy Conversion*, vol. 36, no. 2, pp. 1323–1335, 2020.

[5] Y. Xiang, Q. Li, Y. Li et al., "Twofold symmetry of c-axis resistivity in topological kagome superconductor CsV3Sb5 with in-plane rotating magnetic field," *Nature Communications*, vol. 12, no. 1, pp. 1–8, 2021.

[6] R. Bhattarai, N. Gurung, and S. Kamalasadan, "Dual mode control of a three-phase inverter using minimum variance adaptive architecture," *IEEE Transactions on Industry Applications*, vol. 54, no. 4, pp. 3868–3880, 2018.

[7] Z. Shi, X. Sun, Y. Cai, and Z. Yang, "Robust design optimization of a five-phase PM hub motor for fault-tolerant operation based on taguchi method," *IEEE Transactions on Energy Conversion*, vol. 35, no. 4, pp. 2036–2044, 2020.

[8] H. Saneie, R. Alipour-Sarabi, Z. Nasiri-Gheidari, and F. Tootoonchian, "Challenges of finite element analysis of resolvers," *IEEE Transactions on Energy Conversion*, vol. 34, no. 2, pp. 973–983, 2018.

[9] T. Deng, Z. Su, J. Li, P. Tang, X. Chen, and P. Liu, "Advanced angle field weakening control strategy of permanent magnet synchronous motor," *IEEE Transactions on Vehicular Technology*, vol. 68, no. 4, pp. 3424–3435, 2019.

[10] H. Wei, J. Yu, Y. Zhang, and Q. Ai, "High-speed control strategy for permanent magnet synchronous machines in electric vehicles drives: analysis of dynamic torque response and instantaneous current compensation," *Energy Reports*, vol. 6, pp. 2324–2335, 2020.

[11] M. A. Soliman, H. M. Hasanien, S. Alghuwainem, and A. Al-Durra, "Symbiotic organisms search algorithm-based optimal control strategy for efficient operation of variable-speed wind generators," *IET Renewable Power Generation*, vol. 13, no. 14, pp. 2684–2692, 2019.

[12] C. Lai, G. Feng, J. Tjong, and N. C. Kar, "Direct calculation of maximum-torque-per-ampere angle for interior PMSM control using measured speed harmonic," *IEEE Transactions on Power Electronics*, vol. 33, no. 11, pp. 9744–9752, 2018.

[13] W. Lu, B. Tang, K. Ji, K. Lu, D. Wang, and Z. Yu, "A new load adaptive identification method based on an improved sliding mode observer for PMSM position servo system," *IEEE Transactions on Power Electronics*, vol. 36, no. 3, pp. 3211–3223, 2020.

[14] X. Sun, Y. Cai, S. Wang, X. Xu, and L. Chen, "Optimal control of intelligent vehicle longitudinal dynamics via hybrid model predictive control," *Robotics and Autonomous Systems*, vol. 112, pp. 190–200, 2019.

[15] V. Repecho, J. B. Waqar, D. Biel, and A. Dòria-Cerezo, "Zero speed sensorless scheme for permanent magnet synchronous machine under decoupled sliding-mode control," *IEEE Transactions on Industrial Electronics*, vol. 69, no. 2, pp. 1288–1297, 2021.

[16] K. Li, G. Cheng, X. Sun, Z. Yang, and Y. Fan, "Performance optimization design and analysis of bearingless induction motor with different magnetic slot wedges," *Results in Physics*, vol. 12, pp. 349–356, 2019.

[17] W. Wang, H. Lin, H. Yang, W. Liu, and S. Lyu, "Second-order sliding mode-based direct torque control of variable-flux memory machine," *IEEE Access*, vol. 8, pp. 34981–34992, 2020.

[18] D. Xu, B. Wang, G. Zhang, G. Wang, and Y. Yu, "A review of sensorless control methods for AC motor drives," *CES Transactions on electrical machines and systems*, vol. 2, no. 1, pp. 104–115, 2018.

[19] L. Po, L. Ruiyu, S. Tianying, Z. Jingrui, and F. Zheng, "Composite adaptive model predictive control for DC-DC boost converters," *IET Power Electronics*, vol. 11, no. 10, pp. 1706–1717, 2018.

[20] C. Capasso, D. Lauria, and O. Veneri, "Experimental evaluation of model-based control strategies of sodium-nickel chloride battery plus supercapacitor hybrid storage systems for urban electric vehicles," *Applied Energy*, vol. 228, pp. 2478–2489, 2018.

[21] K. T. Chau, C. C. Chan, and C. Chunhua Liu, "Overview of permanent-magnet brushless drives for electric and hybrid electric vehicles," *IEEE Transactions on Industrial Electronics*, vol. 55, no. 6, pp. 2246–2257, 2008.

[22] J.-Q. Yang, N. Jiang, Z.-P. Li et al., "The effects of microgravity on the digestive system and the new insights it brings to the life sciences," *Life Sciences and Space Research*, vol. 27, pp. 74–82, 2020.

[23] X. Xibo Yuan and J. Jiabin Wang, "Torque distribution strategy for a front- and rear-wheel-driven electric vehicle," *IEEE Transactions on Vehicular Technology*, vol. 61, no. 8, pp. 3365–3374, 2012.